Manuscript accepted for publication at the IJNM Special Issue on
Advances in Simulation-driven Modeling and Optimization of Microwave/RF Circuits



# Design Optimization of Full-Wave EM Models by Low-Order Low-Dimension Polynomial Surrogate Functionals

José E. Rayas-Sánchez, *Senior Member, IEEE*, José L. Chávez-Hurtado, and Zabdiel Brito-Brito, *Member, IEEE*

***Abstract*—A practical formulation for EM-based design optimization of high-frequency circuits using simple polynomial surrogate functionals is proposed in this paper. Our approach starts from a careful selection of design variables and is based on a closed-form formulation that yields global optimal values for the surrogate model weighting factors, avoiding a large set of expensive EM model data, and resulting in accurate low-order low-dimension polynomials interpolants that are used as vehicles for efficient design optimization. Our formulation is especially suitable for EM-based design problems with no equivalent circuital models available. The proposed technique is illustrated by the EM-based design optimization of a Ka-band substrate integrated waveguide (SIW) interconnect with conductor-backed coplanar waveguide (CBCPW) transitions, a low crosstalk PCB microstrip interconnect structure with guard traces, and a 10-40 GHz SIW interconnect with microstrip transitions on a standard FR4-based substrate. Three commercially available full-wave EM solvers are used in our examples: CST, Sonnet and COMSOL.**

***Index Terms*— Surrogate modeling, polynomial functionals, EM-based optimization, space mapping, high-speed interconnects, substrate integrated waveguides, CPW-SIW transitions, guard traces, microstrip-SIW transitions.**

## I. Introduction

Design optimization and statistical analysis of high-frequency structures require in practice the availability of accurate and computationally inexpensive models. Such models can be implemented by surrogates. Originally [1], surrogate modeling refers to the iterative construction of functional relationships between the design space and the performance space based on a limited amount of fine model data (highly accurate but computationally expensive simulations), with no derivatives information available. Engineering applications of surrogate modeling started in geology, aerospace, and chemistry, later being extended to electrical engineering [2].

Many innovative approaches have been proposed in the area of RF and microwave circuits to develop surrogate models. When physics-based coarse models (i.e., low fidelity but computationally inexpensive models) are incorporated in the modeling process, a variety of techniques are available, most of them following space mapping (SM) approaches [3,4], which are known to be very efficient.

However, a reliable physics-based coarse model is not always available for the design task. For instance, many antenna structures [5,6] and SIW interconnects [7,8] do not have parameterized equivalent circuital models. Although a simplified and coarsely discretized full-wave EM model can be used in those cases (with the same solver employed for the fine model), they usually exhibit numerical noise, discontinuous behavior, and non-negligible simulation time with respect to the

J. E. Rayas-Sánchez, J. L. Chávez-Hurtado, and Z. Brito-Brito are with the Department of Electronics, Systems, and Informatics, ITESO – The Jesuit University of Guadalajara, 45604 Mexico (phone +52 33 3669 3598; e-mail: erayas@iteso.mx; website: http://desi.iteso.mx/caecas/).

corresponding original fine model [9]. In this scenario, the surrogate model can be built from directly sampling of the fine model, following a metamodeling approach [10,11]. These surrogate modeling techniques are more general than those based on physics-based coarse models, however, they are more computationally intensive. They include multidimensional quadratic models [12,13], multidimensional Cauchy models [14], linear regression models [15], rational function fitting [16], neural models [17-20], support vector regression [21-23], and non-probabilistic kriging models [24-26].

Among metamodeling approaches, using polynomial surrogates offers the simplest implementation [2]. However, they suffer from a large number of free-parameters or weighting factors when the problem dimensionality is too large or when the problem non-linearity is too high, which implies in both cases a high-order polynomial and a large set of fine model data to develop the surrogate.

Pure polynomial surrogates can be efficiently developed even for highly non-linear problems with a high dimensionality and a large exploration region for the design variables, as long as some decomposition strategy combined with a piece-wise linearization approach is applied [27-30].

In this paper, we demonstrate how polynomial surrogate models offer a simple and effective strategy to optimize expensive EM models through a careful selection of design variables and a systematic closed-form formulation that avoids requiring a large set of fine model data, yielding accurate low-order low-dimension polynomial surrogate functionals. This approach is especially suitable for EM-based design optimization problems with no physics-based coarse models available. Our work improves and extends that one in [31] by presenting: a) a generalized formulation for the *N*th-order polynomial surrogate; and b) an enhanced formulation based on the simultaneous calculation of all the weighting factors available for the *N*th-order surrogate (instead of considering fixed the previously developed lower-order polynomial, as in [31]). We demonstrate how the new formulation yields smaller learning errors and better generalization performance. Our proposed new technique is illustrated by three design optimization cases: 1) a Ka-band substrate integrated waveguide (SIW) interconnect with conductor-backed coplanar waveguide (CBCPW) transitions; 2) a low crosstalk PCB microstrip structure with guard traces; and 3) a 10-40 GHz SIW interconnect with microstrip transitions on a standard FR4-based substrate. Three different commercially available full-wave electromagnetic simulators are employed in our examples: CST, Sonnet and COMSOL.

## II. Original Fine Model and its Surrogate

### *A. Fine Model*

Let $\boldsymbol{R}_f \in \Re^p$ denote a fine model response vector, sampled at $p$ independent-variable points. Response $\boldsymbol{R}_f$ can be at any domain (frequency-domain, time-domain, or static). We consider that $\boldsymbol{R}_f$ depends on three vectors: the selected design variables, $\boldsymbol{x} \in \Re^n$, the pre-assigned model parameters, $\boldsymbol{z} \in \Re^m$, and the fine model simulation conditions, $\boldsymbol{\psi}_f$. Selecting suitable design variables $\boldsymbol{x}$ for a given problem usually requires engineering expertise, while most of the pre-assigned parameters $\boldsymbol{z}$ are usually determined by manufacturing constraints as well as by engineering knowledge about the influence of the physical parameters on the circuit responses of interest. The fine model simulation conditions $\boldsymbol{\psi}_f$ are any required combination of independent parameters according to the nature of the simulation, such as the operating frequencies, resolution,

boundary conditions, simulation box size, etc.

From the design optimization perspective, the fine model is treated as a multidimensional (not necessarily continuous) vector function, $\boldsymbol{R}_\mathrm{f}(\boldsymbol{x}) : X_\mathrm{f} \rightarrow \Re^p$ whose domain is $X_\mathrm{f} \subseteq \Re^n$. Evaluating $\boldsymbol{R}_\mathrm{f}(\boldsymbol{x})$ is computationally expensive. Direct optimization of the fine model using classical optimization methods is prohibitive given its typically high computational cost. It requires solving

$$\boldsymbol{x}_\mathrm{f}^* = \arg \min_{\boldsymbol{x} \in X_\mathrm{f}} U(\boldsymbol{R}_\mathrm{f}(\boldsymbol{x})) \tag{1}$$

where $U$: $\Re^n \rightarrow \Re$ is an objective function expressed in terms of the design specifications, and vector $\boldsymbol{x}_\mathrm{f}^*$ contains the optimal fine model design.

### *B. Surrogate Model*

We want to develop a surrogate model $\boldsymbol{R}_\mathrm{s}(\boldsymbol{x}) : X_\mathrm{s} \rightarrow \Re^p$ that approximates the fine model responses within a region of interest $X_\mathrm{s} \subseteq X_\mathrm{f}$ around a base point $\boldsymbol{x}^{(0)}$. Region $X_\mathrm{s}$ is defined as an $n$-dimensional box whose center is $\boldsymbol{x}^{(0)}$. The size of the region of interest $X_\mathrm{s}$ is defined by a vector $\boldsymbol{\tau} \in \Re^n$ containing the relative deviation for each design variable with respect to its central value. To train the surrogate model, we use $L$ learning base points within $X_\mathrm{s}$, denoted as $\boldsymbol{x}^{(1)}$, $\boldsymbol{x}^{(2)}$, …, $\boldsymbol{x}^{(L)}$. Ideally, we aim at developing a surrogate model such that

$$\boldsymbol{R}_\mathrm{s}(\boldsymbol{x}) = \boldsymbol{R}_\mathrm{f}(\boldsymbol{x}) \text{ for all } \boldsymbol{x} \in X_\mathrm{s} \tag{2}$$

In this paper, surrogate models are based on polynomial functional interpolants whose optimal weighting factors are obtained in closed form.

## III. First-Order Polynomial Surrogate Model

The first-order functional surrogate is selected as

$$\boldsymbol{R}_\mathrm{s}^{(1)}(\boldsymbol{x}) = \boldsymbol{R}_\mathrm{f}(\boldsymbol{x}^{(0)}) + \boldsymbol{W}^{(1)}(\boldsymbol{x} - \boldsymbol{x}^{(0)}) \text{ for all } \boldsymbol{x} \in X_\mathrm{s} \tag{3}$$

where matrix $\boldsymbol{W}^{(1)} \in \Re^{p \times n}$ contains all the first-order surrogate model weighting factors.

The surrogate model response at the $j$-th learning base point $\boldsymbol{x}^{(j)}$ should match the corresponding fine model response, for $j = 1, \ldots L$,

$$\boldsymbol{R}_\mathrm{s}^{(1)}(\boldsymbol{x}^{(j)}) = \boldsymbol{R}_\mathrm{f}(\boldsymbol{x}^{(0)}) + \boldsymbol{W}^{(1)}(\boldsymbol{x}^{(j)} - \boldsymbol{x}^{(0)}) = \boldsymbol{R}_\mathrm{f}(\boldsymbol{x}^{(j)}) \tag{4}$$

Applying (4) at $L$ learning base points, the following linear system is established,

$$\boldsymbol{W}^{(1)} \boldsymbol{\Delta X}^{(1)} = \boldsymbol{\Delta R}^{(0)} \tag{5}$$

where $\boldsymbol{\Delta X}^{(1)} \in \Re^{n \times L}$ and $\boldsymbol{\Delta R}^{(0)} \in \Re^{p \times L}$ are

$$\boldsymbol{\Delta X}^{(1)} = \begin{bmatrix} (\boldsymbol{x}^{(1)} - \boldsymbol{x}^{(0)}) \\ \vdots \\ (\boldsymbol{x}^{(L)} - \boldsymbol{x}^{(0)}) \end{bmatrix}^\mathrm{T} \tag{6}$$

$$\boldsymbol{\Delta R}^{(0)} = \begin{bmatrix} \boldsymbol{R}_\mathrm{f}(\boldsymbol{x}^{(1)}) - \boldsymbol{R}_\mathrm{f}(\boldsymbol{x}^{(0)}) \\ \vdots \\ \boldsymbol{R}_\mathrm{f}(\boldsymbol{x}^{(L)}) - \boldsymbol{R}_\mathrm{f}(\boldsymbol{x}^{(0)}) \end{bmatrix}^\mathrm{T} \tag{7}$$

We find the weighting factors of the first-order polynomial surrogate model by solving (5) in the least squares sense,

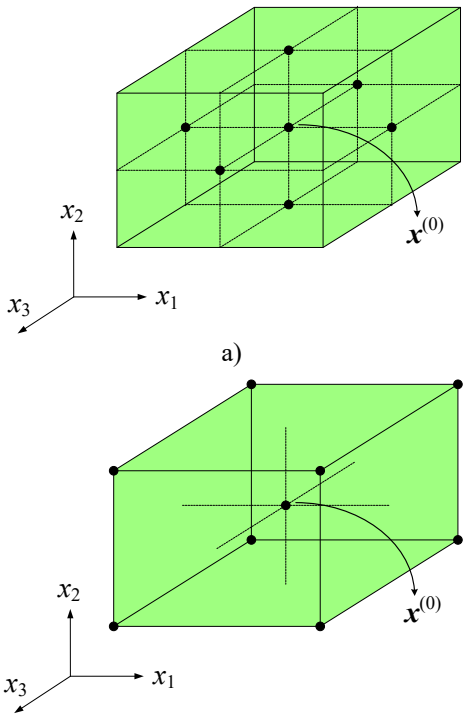


Fig. 1 Distributions of learning base points for a 3-dimensional design problem ($n$ = 3): a) star distribution ($2n$+1 base points), b) box distribution ($2^n$ base points).

$$\boldsymbol{W}^{(1)} = \boldsymbol{\Delta R}^{(0)} (\boldsymbol{\Delta X}^{(1)})^{+} \tag{8}$$

where $(\cdot)^{+}$ denotes the pseudo-inverse. Notice that (8) yields a unique solution (global optimal values for the linear surrogate model weighting factors) even in the case of matrix $\boldsymbol{\Delta X}^{(1)}$ being rank deficient, as long as the corresponding pseudo inverse is calculated using singular value decomposition [32]. However, from (6) it is seen that $\boldsymbol{\Delta X}^{(1)}$ is full-rank for almost any reasonable distribution of learning points; for instance, when we select a star distribution, as in Fig. 1a, a box distribution, as in Fig. 1b, or a uniform distribution.

## IV. Second-Order Polynomial Surrogate

Our second-order functional surrogate is defined as

$$\boldsymbol{R}_{\mathrm{s}}^{(2)}(\boldsymbol{x}) = \boldsymbol{R}_{\mathrm{s}}^{(1)}(\boldsymbol{x}) + \begin{bmatrix} \vdots \\ (\boldsymbol{x} - \boldsymbol{x}^{(0)})^{\mathrm{T}} \boldsymbol{W}_k^{(2)} (\boldsymbol{x} - \boldsymbol{x}^{(0)}) \\ \vdots \end{bmatrix} \tag{9}$$

where matrix $\boldsymbol{W}_k^{(2)} \in \Re^{n \times n}$ contains the weighting factors of the second order terms for the $k$-th independent variable sample, for $k = 1 \ldots p$. In contrast to other quadratic surrogates [33-36], our formulation includes all second order crossed terms.

The free parameters of the second-order surrogate model $\boldsymbol{W}_k^{(2)}$ can be calculated as in [31], by considering that $\boldsymbol{R}_{\mathrm{s}}^{(1)}$ in (9) is already developed, with its parameters already calculated using (8). In this work we follow a better approach, by calculating matrices of weighting factors $\boldsymbol{W}^{(1)}$ and $\boldsymbol{W}_k^{(2)}$ simultaneously, as follows.

The $k$-th surrogate model response at the $j$-th learning base point $\boldsymbol{x}^{(j)}$ should match the corresponding $k$-th fine model response,

$$R_{\mathrm{fk}}(\boldsymbol{x}^{(0)}) + \boldsymbol{w}_k^{(1)\mathrm{T}}(\boldsymbol{x}^{(j)} - \boldsymbol{x}^{(0)}) + (\boldsymbol{x}^{(j)} - \boldsymbol{x}^{(0)})^{\mathrm{T}} \boldsymbol{W}_k^{(2)} (\boldsymbol{x}^{(j)} - \boldsymbol{x}^{(0)}) = R_{\mathrm{fk}}(\boldsymbol{x}^{(j)}) \tag{10}$$

where $j = 1,\ldots, L$ and $\boldsymbol{w}_k^{(1)\mathrm{T}} \in \Re^{1\times n}$ is the $k$-th row of $\boldsymbol{W}^{(1)}$. Applying (10) at $L$ learning base points, the following linear system is established,

$$\boldsymbol{\Delta X}^{(1,2)} \boldsymbol{w}_k^{(1,2)} = \boldsymbol{\Delta R}_k^{(0)} \tag{11}$$

where

$$\boldsymbol{w}_k^{(1,2)} = \left[\boldsymbol{w}_k^{(1)} \quad \boldsymbol{w}_{k1}^{(2)} \quad \boldsymbol{w}_{k2}^{(2)} \quad \ldots \quad \boldsymbol{w}_{kn}^{(2)}\right]^{\mathrm{T}} \in \Re^{(n^2+n)} \tag{12}$$

$$\boldsymbol{\Delta X}^{(1,2)} = \left[\boldsymbol{\Delta X}^{(1)^{\mathrm{T}}} \quad \boldsymbol{\Delta X}^{(2)}\right] \in \Re^{L\times(n^2+n)} \tag{13}$$

$$\boldsymbol{\Delta X}^{(2)} = \begin{bmatrix} (x_1^{(1)} - x_1^{(0)})(\boldsymbol{x}^{(1)} - \boldsymbol{x}^{(0)})^{\mathrm{T}} & \ldots & (x_n^{(1)} - x_n^{(0)})(\boldsymbol{x}^{(1)} - \boldsymbol{x}^{(0)})^{\mathrm{T}} \\ \vdots & \ddots & \vdots \\ (x_1^{(L)} - x_1^{(0)})(\boldsymbol{x}^{(L)} - \boldsymbol{x}^{(0)})^{\mathrm{T}} & \ldots & (x_n^{(L)} - x_n^{(0)})(\boldsymbol{x}^{(L)} - \boldsymbol{x}^{(0)})^{\mathrm{T}} \end{bmatrix} \in \Re^{L\times n^2} \tag{14}$$

$$\boldsymbol{\Delta R}_k^{(0)} = \begin{bmatrix} R_{\mathrm{fk}}(\boldsymbol{x}^{(1)}) - R_{\mathrm{fk}}(\boldsymbol{x}^{(0)})) \\ \vdots \\ R_{\mathrm{fk}}(\boldsymbol{x}^{(L)}) - R_{\mathrm{fk}}(\boldsymbol{x}^{(0)})) \end{bmatrix} \in \Re^{L} \tag{15}$$

with $\boldsymbol{\Delta x}^{(1)}$ defined in (6). Weighting factors (12) of this second-order polynomial surrogate model can be obtained from (11) using

$$\boldsymbol{w}_k^{(1,2)} = (\boldsymbol{\Delta X}^{(1,2)})^{+} \boldsymbol{\Delta R}_k^{(0)} \text{ for } k = 1 \ \ldots \ p \tag{16}$$

Formulation (16) yields a unique solution (global optimal values for the second-order surrogate model weighting factors) as long as the corresponding pseudo-inverse is calculated using singular value decomposition [32].

## V. Higher-Order Polynomial Surrogate Models

Our $N$-th order functional surrogate is defined as

$$\boldsymbol{R}_{\mathrm{s}}^{(N)}(\boldsymbol{x}) = \boldsymbol{R}_{\mathrm{s}}^{(N\text{-}1)}(\boldsymbol{x}) + \begin{bmatrix} \vdots \\ (\boldsymbol{x} - \boldsymbol{x}^{(0)})^{\mathrm{T}} \boldsymbol{W}_k^{(N)} (\boldsymbol{x} - \boldsymbol{x}^{(0)})^{\wedge(N\text{-}1)} \\ \vdots \end{bmatrix} \tag{17}$$

with $k = 1 \ \ldots \ p$. Operator ^ denotes element-wise power, and matrix $\boldsymbol{W}_k^{(N)} \in \Re^{n\times n}$ contains the weighting factors of the $N$-th order term for the $k$-th independent variable sample. Similarly to the second order surrogate, and in contrast to the work in [31], here we obtain all the weighting factors $\boldsymbol{W}^{(1)}$, $\boldsymbol{W}_k^{(2)}$, …, $\boldsymbol{W}_k^{(N)}$ of the $N$-th order surrogate model simultaneously for the $k$-th independent variable sample.

Considering $L$ learning base points, the following linear system is established,

$$\boldsymbol{\Delta X} \boldsymbol{w}_k = \boldsymbol{\Delta R}_k^{(0)} \tag{18}$$

where

$$\boldsymbol{w}_k = \left[\boldsymbol{w}_k^{(1)} \quad \boldsymbol{w}_{k1}^{(2)} \quad \ldots \quad \boldsymbol{w}_{kn}^{(2)} \quad \ldots \quad \boldsymbol{w}_{k1}^{(N)} \quad \ldots \quad \boldsymbol{w}_{kn}^{(N)}\right]^{\mathrm{T}} \tag{19}$$

$$\boldsymbol{\Delta X} = \left[ \boldsymbol{\Delta X}^{(1)\mathrm{T}} \quad \boldsymbol{\Delta X}^{(2)} \quad \ldots \quad \boldsymbol{\Delta X}^{(N)} \right] \tag{20}$$

$$\boldsymbol{\Delta X}^{(N)} = \begin{bmatrix} (x_1^{(1)} - x_1^{(0)})^{N-1} (\boldsymbol{x}^{(1)} - \boldsymbol{x}^{(0)})^{\mathrm{T}} & \ldots & (x_n^{(1)} - x_n^{(0)})^{N-1} (\boldsymbol{x}^{(1)} - \boldsymbol{x}^{(0)})^{\mathrm{T}} \\ \vdots & \ddots & \vdots \\ (x_1^{(L)} - x_1^{(0)})^{N-1} (\boldsymbol{x}^{(L)} - \boldsymbol{x}^{(0)})^{\mathrm{T}} & \ldots & (x_n^{(L)} - x_n^{(0)})^{N-1} (\boldsymbol{x}^{(L)} - \boldsymbol{x}^{(0)})^{\mathrm{T}} \end{bmatrix} \tag{21}$$

with $\boldsymbol{w}_k \in \Re^{(N-1)n^2+n}$, $\boldsymbol{\Delta X} \in \Re^{L\times((N-1)n^2+n)}$, and $\boldsymbol{\Delta X}^{(1)}$, $\boldsymbol{\Delta X}^{(2)}$, and $\boldsymbol{\Delta R}_k^{(0)}$ defined in (6), (14), and (15), respectively. The global optimal set of weighting factors (least squares solution of smallest 2-norm) for the $N$-th order polynomial surrogate model $\boldsymbol{R}_s^{(N)}$ is obtained from (18) using

$$\boldsymbol{w}_k = (\boldsymbol{\Delta X})^{+} \boldsymbol{\Delta R}_k^{(0)} \text{ for } k = 1 \ldots p \tag{22}$$

If the polynomial surrogate is developed over a large training region, or the nonlinearity of the fine model responses with respect the design parameters is too high, high order polynomials might be needed. In our approach, we keep $N \leq 4$. If a higher order polynomial is required, decomposition in the design space can be applied, as mentioned in Section I.

## VI. SIW Interconnect with CBCPW Transitions

As a first example, consider the single-layer substrate integrated waveguide (SIW) interconnect with transitions to conductor-backed coplanar waveguide (CBCPW) proposed in [37]. Its geometry is shown in Fig. 2. The bandpass of this interconnect is intended for the Ka band (26.5-40 GHz). The transition section is designed to match the monomode propagation on the SIW over the entire frequency passband.

A detailed view of the transition structure is shown in Fig. 3. The structure is embedded in a dielectric layer with $\varepsilon_r = 2.94$ and $\tan(\delta) = 0.0012$ at 10 GHz. The substrate height is $H = 20$ mil. The SIW has a width $W_{SIW} = 4.3$ mm. Each via has a diameter $d = 0.3$ mm and is separated from adjacent vias by a center-to-center spacing $s = 2d$. All vias and metallic planes use copper with a conductivity $\sigma_{Cu} = 5.8 \times 10^7$ S/m. Metal planes use a thickness $t = 0.65$ mil (half-ounce copper). The above parameter values were chosen as in [37].

A separate direct EM minimization of $|S_{11}|$ from 0 GHz to 40 GHz was performed for a short and uniform CBCPW line grounded by rows of vias, yielding a signal trace width $W = 0.9$ mm and a slot width $S = 0.2262$ mm. This initial EM optimization is fast given the simplicity of the corresponding structure. We use a distance $g = 0.358$ mm between the outer edge of the slots

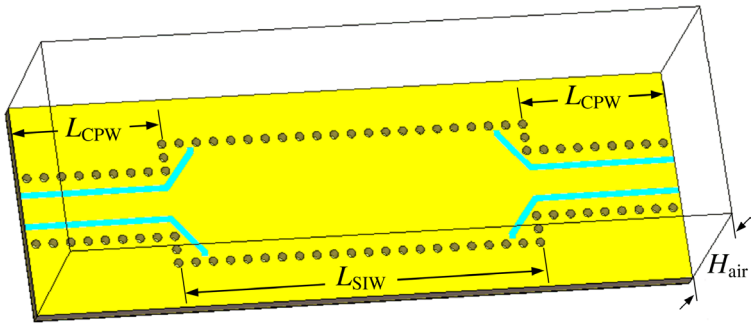


Fig. 2 Single-layer substrate integrated waveguide interconnect (SIW) with transitions to conductor backed coplanar waveguides (CBCPW) with lateral planes grounded by rows vias. From [31].

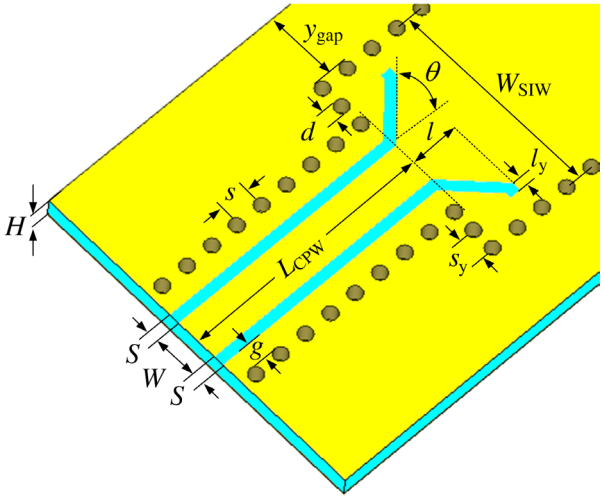


Fig. 3 Detailed view of the transition SIW-CBCPW. From [31].

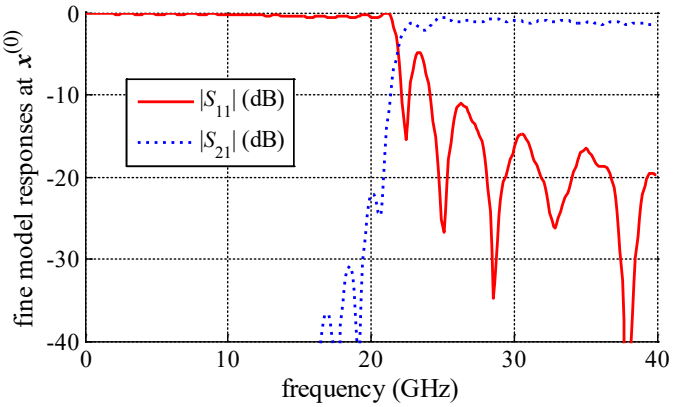


Fig. 4 CST EM responses of the CBPCPW-SIW interconnect at the initial design $\boldsymbol{x}^{(0)}$. From [31]. Intended bandpass range: 26.5-40 GHz.

to the rows of vias on both sides of the CBCPW. These values of $W$, $S$ and $g$ impose $s_y = 0.4085$ mm (see Fig. 3). This selection ensures monomode operation and low leakage characteristics of the coplanar lines. The length of the central conductor is $L_{CPW} = 8.5s = 5.1$ mm ($\approx 5W$). Coplanar tapers and uniform SIW section are on an area whose length is $L_{SIW} = 21s = 12.6$ mm. This length has a sufficient extension for the EM fields to match the dominant mode of propagation within the SIW.

The complete structure is implemented in CST[1]. An air layer whose height is $H_{air} = 10H$ separates the structure from the top cover (see Fig. 2) which was defined as an open wall. A distance $y_{gap} = 1.66$ mm separates the SIW from the bounding box lateral walls. First-order Debye model is used in CST for substrate dispersion.

The impedance of the transition can be effectively tuned by varying the angle $\theta$ and the length of the linear taper $l$ (see Fig. 3). The design space is limited by geometrical constrains mainly associated with the position of the row of vias. For instance, the angle $\theta$ cannot be equal (or close) to 90° as this needs for an extended length of the central conductor, $L_{CPW}$, beyond the transversal rows of vias positioned on both sides of the CBCPW. This extended section of the

[1] CST Microwave Studio, CST AG, Darmstadt, Germany.

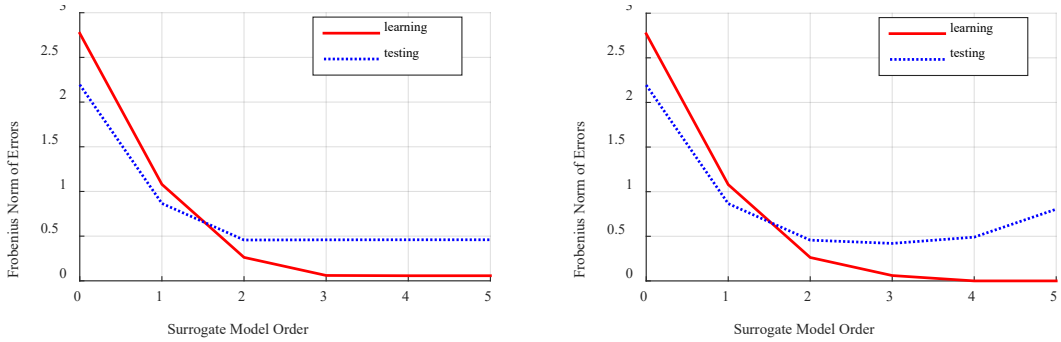


a) b)

Fig. 5 Evolution of the Frobenius norm of the matrix of learning and testing errors for the surrogate models of $|S_{11}|$ of the CBPCPW-SIW interconnect, using: a) formulation in [31]; b) new formulation (22).

coplanar line would create a large separation from the rows of vias on the SIW area, giving rise to unwanted waveguide modes of propagation. Therefore, smaller aperture angles in the taper line are used. A stub length $l_y$ = 0.2 mm allows an adequate variation of the angle and length for impedance tuning (see Fig. 3). Based on [37], an angle $\theta$ = 45° and a length $l$ = 1 mm for the linear taper were initially chosen. EM responses at the initial design are displayed in Fig. 4. CST field solver required five adaptive passes (starting with 10 lines per waveguide and ending up with 35 lines per wavelength) to ensure resolution mesh convergence.

### *A. Surrogate Modeling of the SIW-CBCPW Structure*

We select as design parameters $\boldsymbol{x} = [\theta\,(\text{degrees}) \quad l\,(\text{mm})]^T$ to build a polynomial surrogate model. Our initial design uses $\boldsymbol{x}^{(0)} = [45 \quad 1]^T$ whose corresponding fine model response is in Fig. 4. We generate 8 learning base points around $\boldsymbol{x}^{(0)}$, using a ±15% deviation for $\theta$ and ±5% deviation for $l$. To test the generalization performance we use the same 10 random test points used in [31] within this region.

We apply our new surrogate modeling formulation (22) to this problem. The evolution of the Frobenius norm of the matrix of learning and testing errors for the surrogate models of $|S_{11}|$ is shown in Fig. 5. It is seen that, for these amount of learning data, the best results are obtained with a cubic surrogate model, $\boldsymbol{R}_s^{(3)}$. It is also seen that the learning errors are effectively made zero using our new formulation (22) as we increase the order of the surrogate model, in contrast with the results presented in [31], yielding also a better generalization performance for the best surrogate (in this case, a third order surrogate).

Initial and final generalization errors are shown in Fig. 6 for the surrogate model of $|S_{11}|$ (surrogate model of $|S_{21}|$ has a similar behavior).

### *B. Surrogate Model Optimization and Fine Model Validation*

We now optimize $\boldsymbol{R}_s^{(3)}(\boldsymbol{x})$ to minimize $|S_{11}|$ in the Ka band, using a conventional direct search method [38] to solve

$$\boldsymbol{x}_s^* = \arg\min_{\boldsymbol{x}} U(\boldsymbol{R}_s^{(3)}(\boldsymbol{x})) \tag{23}$$

where $U$: $\Re^n \rightarrow \Re$ is a minimax objective function with specifications $|S_{11}| < 0.1$ for 26.5 GHz $\leq f \leq$ 40 GHz.

After 53 surrogate model evaluations (3 seconds for the complete optimization), the optimal solution found is $\boldsymbol{x}_s^* = [49.994 \quad 1.023]^T$. Surrogate model responses before and after

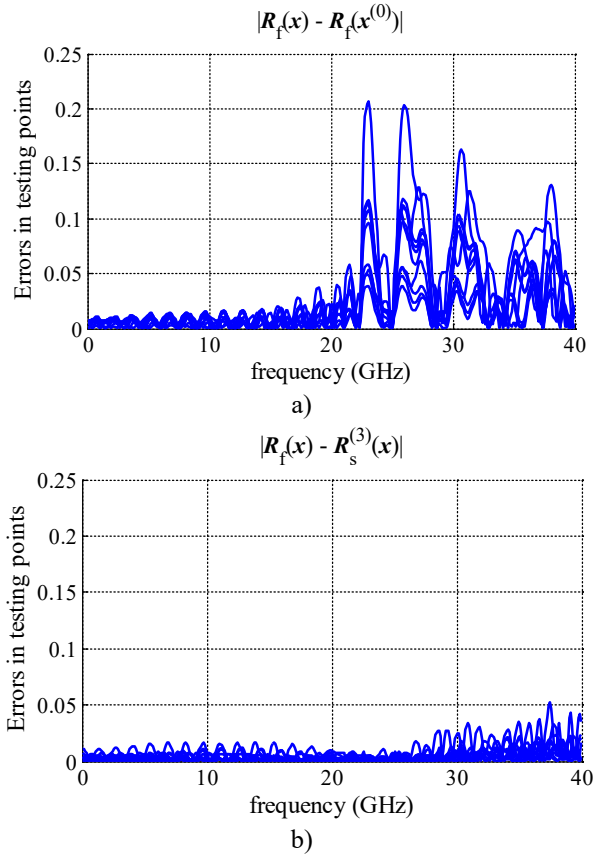


Fig. 6 Absolute errors in $|S_{11}|$ at testing base points, generated by: a) zero-order surrogate, b) third order surrogate obtained from new formulation (22).

optimization are shown in Fig. 7. In Fig. 8 we validate the surrogate solution by comparing the fine and surrogate model responses at $\boldsymbol{x}_s^*$, observing an excellent match between both models.

Finally, fine model response at the starting point and at the optimal surrogate model design are compared in Fig. 9. It is seen from Fig. 9 that the CST fine model response at the optimal surrogate model design $\boldsymbol{x}_s^*$ exhibits a significant reduction in the amount of reflections with respect to the original design within the intended pass-band range (26.5-40 GHz). A similar enhancement is achieved for $|S_{21}|$ (results not shown).

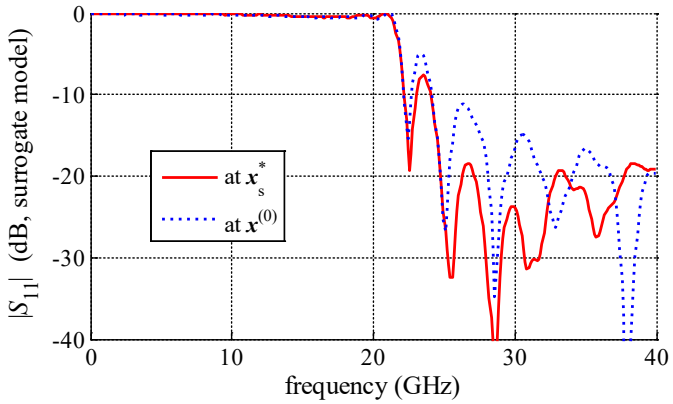


Fig. 7 Polynomial surrogate model response before and after direct optimization of $|S_{11}|$.

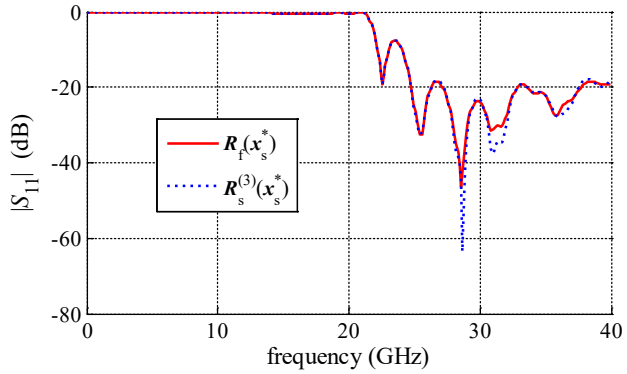


Fig. 8 Comparing the fine and surrogate model responses at $\boldsymbol{x}_s^*$. It is confirmed an excellent match between both models.

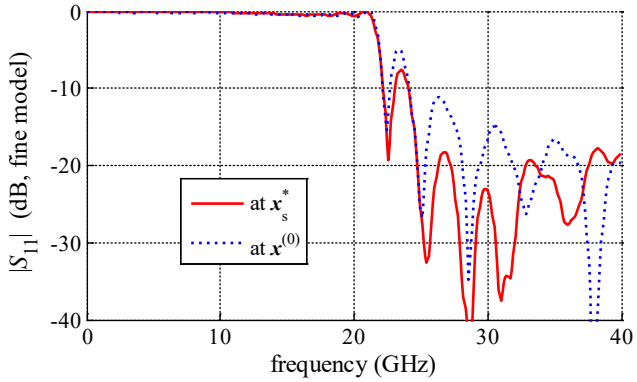


Fig. 9 CST EM fine model responses at the starting point $\boldsymbol{x}^{(0)}$ and at the optimal surrogate model design $\boldsymbol{x}_s^*$. Bandpass range: 26.5-40 GHz.

## VII. Microstrip Traces with Via Fences

As a second example, consider the couple of parallel microstrip traces with an intermediate via fence illustrated in Fig. 10. The usage of guard traces or via fences is a traditional technique to

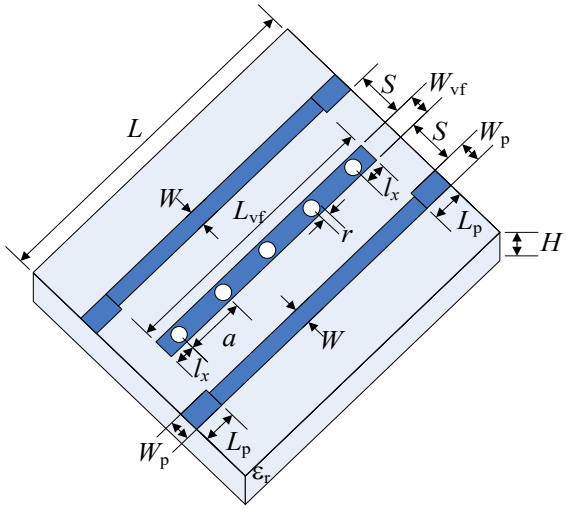


Fig. 10 Microstrip traces with via fence ($W$ is optimized to improve impedance matching, keeping fixed $W_p$ to achieve 50-Ω microstrip lines). From [43].

minimize crosstalk between adjacent microstrip lines on PCBs. It has been demonstrated, both experimentally and by full-wave EM simulations, that inserting via fences between microstrip lines effectively reduces crosstalk [39,40] as well as transmission losses [41]. These benefits, however, usually imply a significant increase in the amount of reflections at the signaling microstrip lines due to deterioration of impedance matching [42]. Here we follow our work in [43] to achieve the above benefits without introducing a significant mismatch, comparing also the performance of the proposed new formulation to train the corresponding surrogate models versus that one used in [31].

The structure uses an FR4 dielectric with a relative permittivity $\varepsilon_r = 4.4$ and a loss tangent $\tan(\delta) = 0.02$ at 10 GHz. The substrate height is $H = 1.575$ mm. The spacing between the microtrip lines and the via fence is $S = 0.75$ mm. Via fence has a width $W_{vf} = 2$ mm, and it contains 25 vias. Each via has a radius $r = 0.762$ mm and is separated from its neighboring via by a center-to-center spacing $a = 4$ mm. The spacing between the center of the extreme vias and the edge of the microstrip lines, in the longitudinal direction, is $l_x = 1.25$ mm (see Fig. 10). The corresponding via fence length is $L_{vf} = 98.5$ mm. All of these parameter values are selected as in [41], excepting for the width of the signaling microstrip traces which is fixed at $W_p = 2.9$ mm (to achieve 50-Ω microstrip lines according to simulations in Sonnet using a very high resolution grid).

To compensate for impedance matching deterioration caused by the guard trace, we make an optimization variable the width of the microstrip lines adjacent to the via fence, $\boldsymbol{x} = W$ (see Fig. 10), and apply our polynomial surrogate approach taking as the initial design $\boldsymbol{x}^{(0)} = W_p$.

The structure is implemented in Sonnet[2] using a very high grid resolution [43]. We show in Fig. 11 the EM responses at the initial design, as well as the structure EM responses with no via

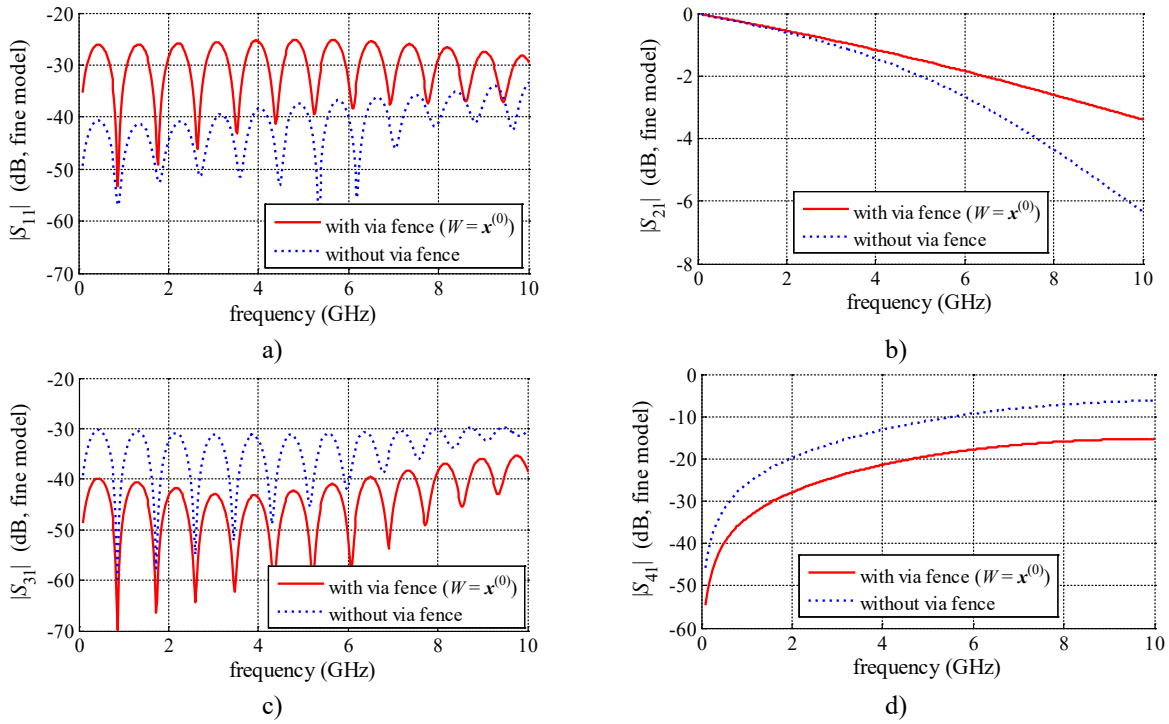


Fig. 11 Sonnet fine model results for microstrip traces with via fence at the initial design and without via fence: a) reflections; b) transmission; c) near-end crosstalk; d) far-end crosstalk. From [43]. It is seen that the uncompensated via fence enhances transmission and reduces crosstalk, at the expense of increasing reflections.

[2] Sonnet Suites™ v12.52, Sonnet Software Inc., North Syracuse, NY.

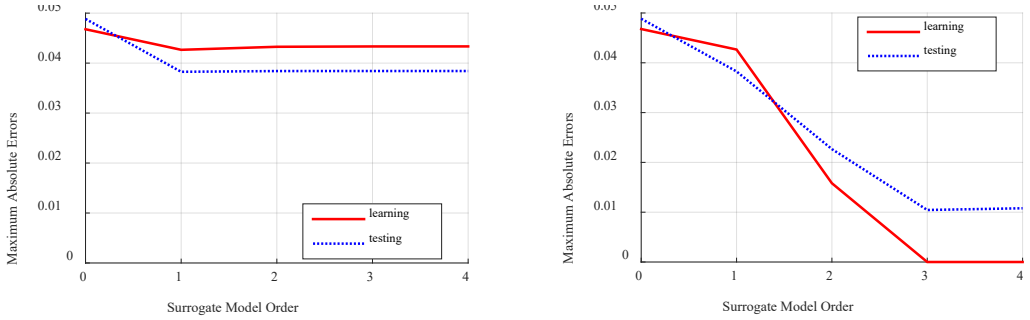


Fig. 12 Evolution of the maximum absolute error of the surrogate models for $|S_{11}|$ of the microstrip traces with via fence, using: a) formulation in [31]; b) new formulation (22).

fence. It is confirmed that both near-end and far-end crosstalk are significantly reduced, as well as the transmission losses, due to the introduction of the via fence. However, a very significant deterioration in the impedance matching of the signaling microstrip lines is observed.

### *A. Surrogate Model of the Microstrip Traces with Via Fence*

We now develop a surrogate model of the structure in Fig. 10 for $|S_{11}|$ as a function of $W$. The region of interest is defined by a tolerance $\tau = -13.79\%$ (2.5 mm $\leq W \leq$ 2.9 mm = $W_p$). To calculate the weighting factors we only use 3 learning base points within this region, and to control

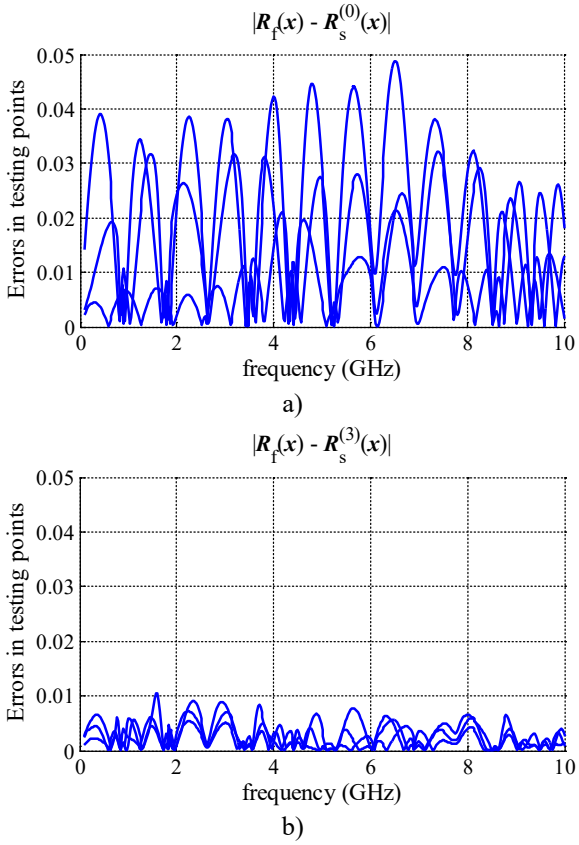


Fig. 13 Generalization errors of the surrogate models for $|S_{11}|$ for the microstrip traces with via fence: a) zero-order model ($\boldsymbol{R}_s^{(0)}(\boldsymbol{x}) = \boldsymbol{R}_f(\boldsymbol{x}^{(0)})$), b) 3rd-order polynomial. From [43].

the generalization performance of the surrogates we use 3 testing points.

Fig. 12 shows the evolution of the maximum absolute error of the surrogates, as we increase their order, with respect to the fine model. It is seen that formulation in [31] has a deficient performance due to insufficient degrees of freedom in the corresponding surrogates (one-dimensional problem with lower-order surrogates fixed), while the proposed formulation (22) is able to make zero the learning errors and yields much better generalization performance. It is also seen in Fig. 12 that the best generalization performance using (22) is achieved by the third-order surrogate, $\boldsymbol{R}_s^{(3)}$. Initial and final generalization errors are shown in Fig. 13.

### *B. Surrogate Optimization and Fine Model Validation*

We now optimize $\boldsymbol{R}_s^{(3)}(\boldsymbol{x})$ to minimize $|S_{11}|$ with respect to $\boldsymbol{x}$ from 0.2 GHz to 9.8 GHz. We apply the sequential quadratic programming (SQP) method available in Matlab[3] to solve (23) using minimax objective function formulation, finding the optimal surrogate model solution $\boldsymbol{x}_s^* = 2.77$ mm. The surrogate model responses before and after optimization are shown in Fig. 14, confirming a significant improvement in the return loss.

In Fig. 15 we compare the fine and surrogate model responses at $\boldsymbol{x}_s^*$, confirming an excellent match between the two models.

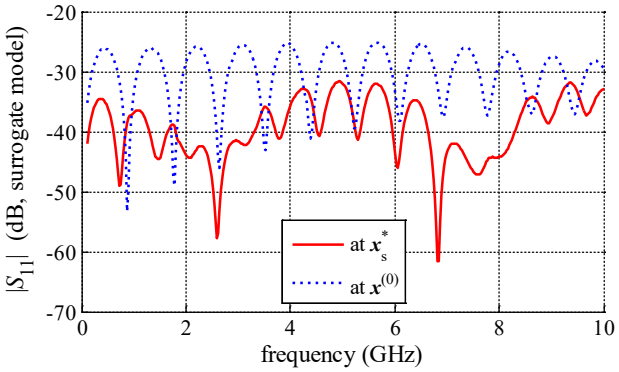


Fig. 14 Cubic surrogate model $\boldsymbol{R}_s^{(3)}$ response at the starting point $\boldsymbol{x}^{(0)}$ and at the optimal surrogate solution $\boldsymbol{x}_s^*$. From [43].

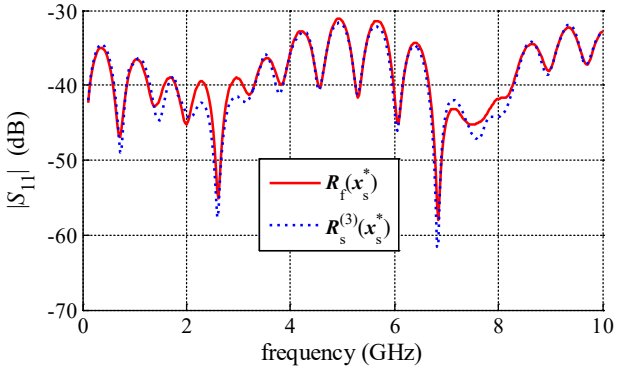


Fig. 15 Fine model response and cubic surrogate model response at the optimal surrogate solution. From [43].

[3] MATLAB, The MathWorks, Inc., 3 Apple Hill Drive, Natick MA 01760-2098.

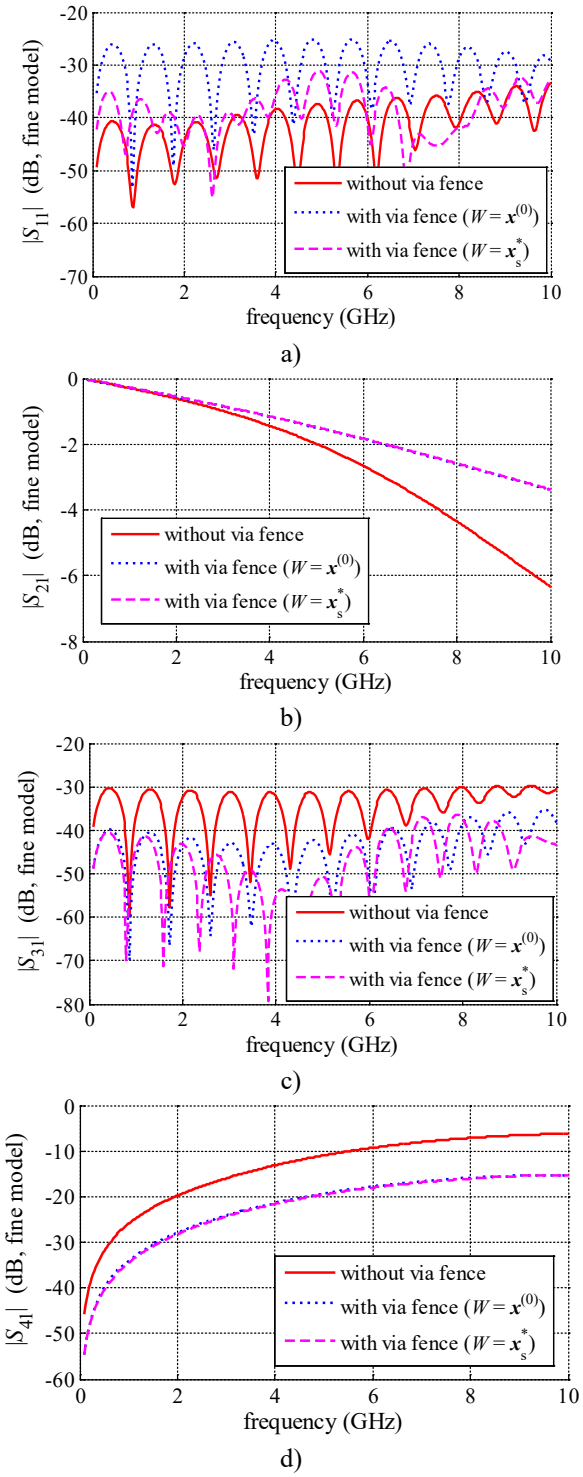


Fig. 16 Sonnet EM responses for microstrip traces without via fence, and with via fence at the initial design and at optimal surrogate solution found. From [43].

The complete fine model responses at $\boldsymbol{x}_s^*$ are shown in Fig. 16 and they are compared with those in Fig. 11. It is confirmed that almost the original reduction of crosstalk and transmission losses is achieved without a significant deterioration of impedance matching, as intended.

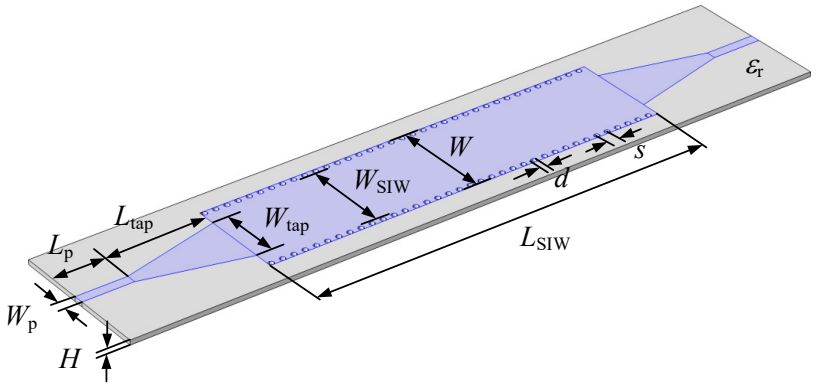


Fig. 17 Single-layer substrate integrated waveguide interconnect (SIW) with microstrip transitions.

## VIII. SIW Interconnect with Microstrip Transitions

As a third example, consider the single-layer substrate integrated waveguide (SIW) interconnect with microstrip transitions proposed in [7]. Its geometry is shown in Fig. 17. The tapered microstrip transition is intended to simultaneously perform field conversion and impedance matching of the two dissimilar guiding structures [8]. The SIW is embedded in a dielectric layer with height $H = 16$ mil, and relative dielectric constant $\varepsilon_r = 3.6$. The SIW waveguide length is $L_{SIW} = 4W$ and has an external width $W = 379.71$ mil. Each via has a diameter $d = 18.9$ mil and is separated from its neighboring via by a center-to-center spacing $s = 2d$. The required cutoff frequency for the dominant mode is $f_{c10} = 10$ GHz, for which the SIW width is $W_{SIW} = 341.91$ mil [7]. The width of the 50-Ω microstrip line is $W_p = 34.14$ mil and its length is $L_p = 1.5W$. The initial transition uses $L_{tap} = 3W$ and $W_{tap} = W_{SIW}$. The above parameter values are chosen as in [7].

The structure is implemented in COMSOL[4]. Our model neglects dielectric and metallic losses by setting $\tan(\delta) = 0$ and by setting all metals as perfect electric conductors (PEC). The simulation bounding box is configured as scattering boundary condition excepting for the bottom cover which is configured as PEC to act as a ground plane. We use in COMSOL model a meshing

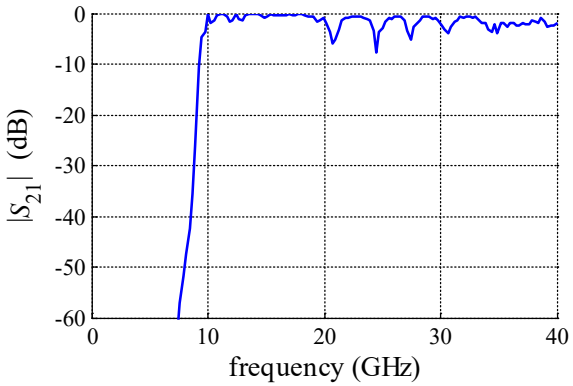


Fig. 18 EM transmission response of the SIW interconnect with transitions to microstrip lines at the initial design $\boldsymbol{x}_f^{(0)} = W_{tap}^{(0)} = W_{SIW}$.

[4] COMSOL Multiphysics version 4.4, 2014, COMSOL AB, Tegnérgatan 23, SE-111 40 Stockholm, Sweden.

scheme by zones, as proposed in [44], using different meshing sizes for different domains in the geometrical model. The distances from the SIW metals to the lateral ($y_{gap}$), frontal ($x_{gap}$) and upper ($H_{air}$) box walls can interfere and modify the EM response of the structure if they are too short. We use $H_{air} = 12H$, $y_{gap} = x_{gap} = 10H$ as proposed in [45]. By using this configuration for the simulation bounding box we ensure not altering the inherent EM response of the structure under analysis [45].

The insertion loss EM response at the initial design is shown in Fig. 18. It is seen that transmission is significantly deteriorated due to the initially selected tapered width $W_{tap} = W_{SIW}$, intended to achieve electromagnetic field match between the two interconnects. This confirms that deficient transitions can excite higher-order modes along the SIW [46], which deteriorate the signal integrity of transmitted digital data and reduce the effective channel bandwidth.

### *A. Surrogate Modeling of the SIW Structure with Microstrip Transitions*

To overcome the above transmission problem, we develop a polynomial surrogate model for $|S_{21}|$ as a function of $W_{tap}$ centered at the average width between the SIW and the microstrip line widths, $W_{avg} = (W_{SIW}+W_p)/2 = 188.025$ mil, over a tolerance region of $\tau = \pm 25$ % (141.02 mil $\leq W_{tap} \leq$ 235.03 mil). To calculate the surrogate model weighting factors we only use 4 learning base points within this region, and to control the generalization performance of the surrogates we use 4 testing points, all uniformly distributed. To illustrate the variability of the transmission response within this region, Fig. 19 shows the fine model responses at the learning and testing base points. Fig. 20 shows the evolution of the Frobenius norm of the learning and testing errors of the surrogates, as we increase their order, with respect to the fine model. It is reconfirmed in this case

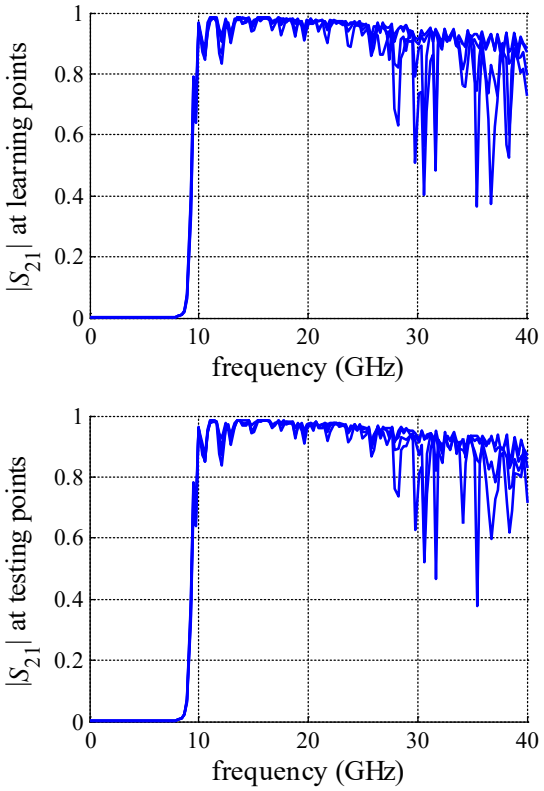


Fig. 19 EM transmission responses of the SIW with transitions to microstrip lines at the learning and testing points in a tolerance region $\tau = \pm 25\%$ for $W_{tap}$ centered at $W_{avg} = (W_{SIW}+W_p)/2$.

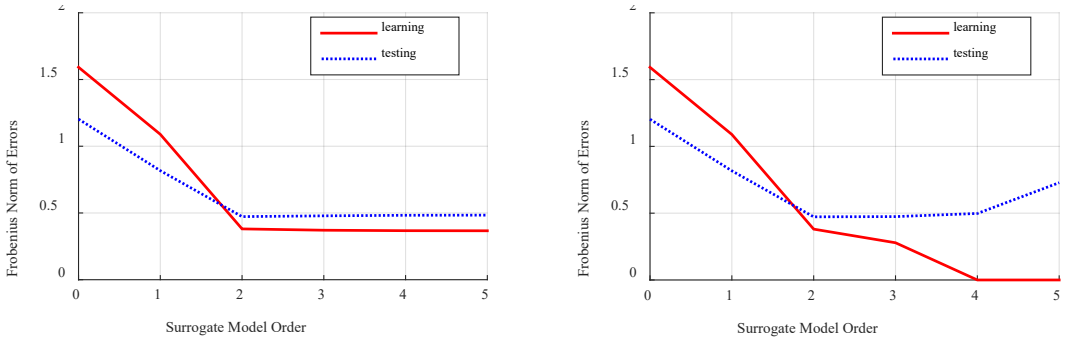


a) b)

Fig. 20 Evolution of the Frobenius norm of the matrix of learning and testing errors for the surrogate models of $|S_{21}|$ for the SIW interconnect with microstrip transitions, using: a) formulation in [31]; b) proposed formulation (22).

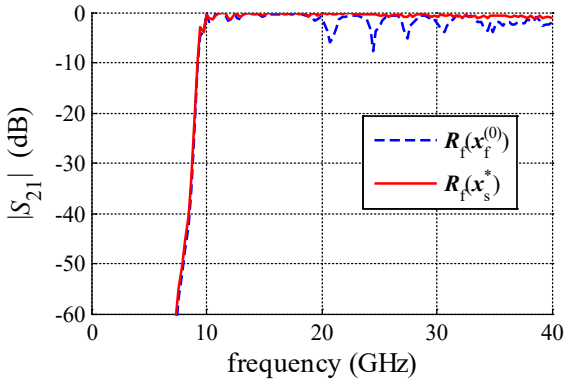


Fig. 21 COMSOL EM transmission responses of the SIW interconnect with transitions to microstrip lines at the initial design $\boldsymbol{x}_f^{(0)} = W_{tap}^{(0)} = W_{SIW}$, and at the optimal surrogate model solution $\boldsymbol{x}_s^*$.

that formulation in [31] is not able to make zero the learning errors as the order of the polynomial surrogates is increased. It is also seen in Fig. 20 that the best generalization performance with formulation (22) is achieved by the second-order surrogate, $\boldsymbol{R}_s^{(2)}$.

### *B. Surrogate Model Optimization and Fine Model Confirmation*

We now optimize $\boldsymbol{R}_s^{(2)}(\boldsymbol{x})$ to improve $|S_{21}|$ in the passband frequency range, solving

$$\boldsymbol{x}_s^* = \arg\min_{\boldsymbol{x}} U(\boldsymbol{R}_s^{(2)}(\boldsymbol{x})) \tag{24}$$

by the SQP method, where $U$: $\Re \rightarrow \Re$ is a minimax objective function with specifications $|S_{21}| > 0.85$ for 12 GHz $\leq f \leq$ 40 GHz. We found the optimal surrogate model solution $\boldsymbol{x}_s^* = 222.37$ mil in 17 surrogate model evaluations, which takes less than a second. Finally, in Fig. 21 we compare the fine model response at the starting point and at the optimal surrogate model design, confirming a very significant improvement in the insertion loss of the SIW interconnect.

## IX. CONCLUSIONS

We presented a practical yet simple EM-based design optimization procedure using low-order low-dimension polynomial functional surrogates. It uses a formulation that yields global optimal weighting factors obtained in closed form, exhibiting smaller learning errors and better generalization performance with respect to a prior formulation. The proposed method is especially suited when no coarse model is available for the problem in hand. Our EM-based design optimization technique as illustrated by several high-speed interconnect examples using three different commercially available EM simulators.

## REFERENCES

[1] A. J. Booker, J. E. Dennis Jr., P. D. Frank, D. B. Serafini, V. Torczon and M. W. Trosset, "A rigorous framework for optimization of expensive functions by surrogates," *Structural Optimization*, vol. 17, pp. 1–13, Feb. 1999.

[2] M. B. Yelten, T. Zhu, S. Koziel, P. D. Franzon, and M. B. Steer, "Demystifying surrogate modeling for circuits and systems," *IEEE Circuits and Systems Magazine*, vol. 12, pp. 45-63, First Quarter 2012.

[3] J. W. Bandler, Q. Cheng, S. A. Dakroury, A. S. Mohamed, M. H. Bakr, K. Madsen and J. Søndergaard, "Space mapping: the state of the art," *IEEE Trans. Microwave Theory Tech.*, vol. 52, pp. 337-361, Jan. 2004.

[4] S. Koziel, Q. S. Cheng and J. W. Bandler, "Space mapping," *IEEE Microwave Magazine*, vol. 9, pp. 105-122, Dec. 2008.

[5] H. Schantz, *The Art and Science of Ultrawideband Antennas*. Boston, MA: Artech House, 2005.

[6] H. Kogure, Y. Kogure, and J. C. Rautio, *Introduction to Antenna Analysis Using EM Simulators*. Tokyo, Japan: Artech House, 2011.

[7] J. E. Rayas-Sánchez and J. A. Jasso-Urzúa, "EM-based optimization of a single layer SIW with microstrip transitions using linear output space mapping," in *IEEE MTT-S Int. Microwave Symp. Dig*., Boston, MA, Jun. 2009, pp. 525-528.

[8] S. Ogurtsov, S. Koziel and J. E. Rayas-Sánchez, "Design optimization of a broadband microstrip-to-SIW transition using surrogate modeling and adaptive design specifications," in *Int. Review of Progress in Applied Computational Electromagnetics (ACES 2010)*, Tampere, Finland, Apr. 2010, pp. 878-883.

[9] S. Koziel and L. Leifsson, Ed., *Surrogate-Based Modeling and Optimization: Applications in Engineering*, New York, NY: Springer, 2013.

[10] T. W. Simpson, J. Peplinski, P. N. Koch, and J. K. Allen, "Metamodels for computer-based engineering design: survey and recommendations," *Engineering with Computers*, vol.17, no. 2, pp. 129-150, Jul. 2001.

[11] G. Wang and S. Shan, "Review of metamodeling techniques in support of engineering design optimization," *Journal Mechanical Design*, vol. 129, pp. 370-380, 2007.

[12] J. W. Bandler, R. M. Biernacki, S. H. Chen, P. A. Grobelny and S. Ye, "Yield-driven electromagnetic optimization via multilevel multidimensional models," *IEEE Trans. Microwave Theory Tech*., vol. 41, pp. 2269-2278, Dec. 1993.

[13] J. W. Bandler, R. M. Biernacki, S. H. Chen and P. A. Grobelny, "A CAD environment for performance and yield driven circuit design employing electromagnetic field simulators," *Proc. IEEE Int. Symp. Circuits Syst.* (London, England), 1994, vol. 1, pp. 145-148.

[14] S. F. Peik, R. R. Mansour, and Y. L. Chow, "Multidimensional Cauchy method and adaptive sampling for an accurate microwave circuit modeling," *IEEE Trans. Microw. Theory Tech.*, vol. 46, no. 12, pp. 2364–2371, Dec. 1998.

[15] G. Doménech-Asensi, J. Hinojosa, J. Martínez-Alajarín and J. Garrigós-Guerrero, "Empirical model generation techniques for planar microwave components using electromagnetic linear regression models," *IEEE Trans. Microwave Theory Tech*., vol. 53, pp. 3305-3311, Nov. 2005.

[16] S. J. Moon and A. C. Cangellaris, "Rational function fitting of electromagnetic transfer functions from frequency-domain and time-domain data," in *IEEE MTT-S Int. Microwave Symp. Dig.*, San Francisco, CA, Jun. 2006, pp. 1609-1612.

[17] A. H. Zaabab, Q. J. Zhang and M. S. Nakhla, "A neural network modeling approach to circuit optimization and statistical design," *IEEE Trans. Microwave Theory Tech*., vol. 43, pp. 1349-1358, Jun. 1995.

[18] P. Burrascano, M. Dionigi, C. Fancelli and M. Mongiardo, "A neural network model for CAD and optimization of microwave filters," in *IEEE MTT-S Int. Microwave Symp. Dig.*, Baltimore, MD, Jun. 1998, pp. 13-16.

[19] Q. J. Zhang and K. C. Gupta, *Neural Networks for RF and Microwave Design*. Norwood, MA: Artech House, 2000.
[20] W. T. Beyene, "Application of artificial neural networks to statistical analysis and nonlinear modeling of high-speed interconnect systems," *IEEE Trans. CAD IC Sys.*, vol. 26, pp. 166-176, Jan. 2007.
[21] L. Xia, J. Meng, R. Xu, B. Yan, and Y. Guo, "Modeling of 3-D vertical interconnect using support vector machine regression," *IEEE Microwave Wireless Compon. Lett*., vol. 16, no. 12, pp. 639-641, Dec. 2006.
[22] G. Angiulli, M. Cacciola, and M. Versaci, "Microwave devices and antennas modelling by support vector regression machines," *IEEE Trans. Magn.*, vol. 43, no. 4, pp. 1589-1592, Apr. 2007.
[23] J. Meng and L. Xia, "Support-vector regression model for millimeter wave transition," *Int. J. Infrared Milimeter Waves*, vol. 28, no. 5, pp. 413-421, May 2007.
[24] L. Lebensztajn, C. Rondini-Marretto, M. Caldora-Costa, and J. L. Coulomb, "Kriging: a useful tool for electromagnetic device optimization," *IEEE Trans. Magnetics*, vol. 40, pp. 1196-1199, Mar. 2004.
[25] S. Koziel, L. Leifsson, I. Couckuyt, and T. Dhaene, "Reliable reduced cost modeling and design optimization of microwave filters using co-kriging," *Int. J. Numerical Modelling-Electronic Networks Devices and Fields*, vol. 26, pp. 493-505, Sep. 2013.
[26] S. Koziel, S. Ogutsov, I. Couckuyt, and T. Dhaene, "Variable-fidelity electromagnetic simulations and co-kriging for accurate modeling of antennas," *IEEE Trans. Antennas Propagation*, vol. 61, pp. 1301-1308, Mar. 2013.
[27] Z. Zhou, Y. S. Ong, M. H. Nguyen, and D. Lim, "A study on polynomial regression and Gaussian process global surrogate model in hierarchical surrogate-assisted evolutionary algorithm," in *IEEE Congress Evolutionary Computation*, Edinburg, Scotland, Sep. 2005, vol. 3, pp. 2832-2839.
[28] H. Filiol, I. O'Connor, and D. Morche, "A new approach for variability analysis of analog ICs," in *Joint IEEE North-East Workshop on Circuits Syst. and TAISA Conf. (NEWCAS-TAISA '09)*, Toulouse, France, Jun. 2009, pp. 1-4.
[29] H. Filiol, I. O'Connor, and D. Morche, "Piecewise-polynomial modeling for analog circuit performance metrics," in *Proc. IEEE European Conf. Circuit Theory and Design (ECCTD)*, Antalya, Turkey, Aug. 2009, pp. 237-240.
[30] H. Filiol, I. O'Connor, and D. Morche, "Analog IC variability bound estimation using the Cornish–Fisher expansion" *IEEE Trans. Comput.-Aided Design Integr. Circuits Syst.*, vol. 31, no. 9, pp. 1457-1461, Sep. 2012.
[31] J. E. Rayas-Sánchez, J. Aguilar-Torrentera and J. A. Jasso-Urzúa, "Surrogate modeling of microwave circuits using polynomial functional interpolants," in *IEEE MTT-S Int. Microwave Symp. Dig*., Anaheim, CA, May 2010, pp. 197-200.
[32] G. W. Stewart, *Introduction to Matrix Computations*. San Diego, CA: Academic Press, 1973.
[33] S. Koziel, "Multi-fidelity multi-grid design optimization of planar microwave structures with Sonnet," in *Int. Review of Progress in Applied Computational Electromagnetics (ACES 2010)*, Tampere, Findland, Apr. 2010, pp. 719-724.
[34] S. Koziel, "Computationally efficient multi-fidelity multi-grid design optimization of microwave structures," *ACES Journal*, vol. 25, no. 17, pp. 578-586, Jul. 2010.
[35] S. Koziel and S. Ogurtsov, "Robust multi-fidelity simulation-driven design optimization of microwave structures", in *IEEE MTT-S Int. Microwave Symp. Dig*., Anaheim, CA, May 2010, pp 201-204.
[36] S. Koziel and S. Ogurtsov, "CPU-budget-driven automated microwave design optimization using variable-fidelity electromagnetic simulations" in *IEEE MTT-S Int. Microwave Symp. Dig*., Montreal, Canada, Jun. 2012, pp. 1-3.
[37] X. Chen and K. Wu, "Low-loss ultra-wideband transition between conductor-backed coplanar waveguide and substrate integrated waveguide", in *IEEE MTT-S Int. Microwave Symp. Dig*., Boston, MA, June 2009, pp 349-352.
[38] J. C. Lagarias, J. A. Reeds, M. H. Wright and P. E. Wright, "Convergence properties of the Nelder-Mead simplex method in low dimensions," *SIAM J. of Optimization*, vol. 9, number 1, pp. 112-147, 1998.
[39] L. Zhi, W. Qiang and S. Changsheng, "Application of guard traces with vias in the RF PCB layout," in *Proc. Int. Symp. Electromagnetic Compatibility*, Minneapolis, MN, May 2002, pp. 771-774.
[40] I. Novak, B. Eged and L. Hatvani, "Measurement and simulation of crosstalk reduction by discrete discontinuities along coupled PCB traces," *IEEE Trans. Inst. Meas.*, vol. 43, pp. 170–175, Apr. 1994.
[41] A. Suntives, A. Khajooeizadeh, R. Abhari, "Using via fence for crosstalk reduction in PCB circuits," in *IEEE Int. Symp. Electromagnetic Compatibility*, Montreal, Quebec, Aug. 2006, pp. 34-37.
[42] R. Sharma, T. Chakravarty and B. A. Bhattacharyya, "Analytical model for optimum signal integrity in PCB interconnects using ground tracks," *IEEE Trans. Electromagnetic Compatibility*, pp. 67-77, vol. 51, Feb. 2009.

[43] J. E. Rayas-Sánchez and N. Vargas-Chávez, "Design optimization of microstrip lines with via fences through surrogate modeling based on polynomial functional interpolants," in *IEEE Conf. Electrical Performance of Electronic Packaging and Systems (EPEPS 2010)*, Austin, TX, Oct. 2010, pp. 125-128.

[44] Z. Brito-Brito, J. E. Rayas-Sánchez, J. C. Cervantes-González, and C. A. López, "Impact of 3D EM model configuration on the direct optimization of microstrip structures," in *COMSOL Conf.*, Boston, MA, Oct. 2013, pp. 1-5.

[45] J. L. Chavez-Hurtado, J. E. Rayas-Sánchez, and Z. Brito-Brito, "Reliable full-wave EM simulation of a single-layer SIW interconnect with transitions to microstrip lines," in *COMSOL Conf.*, Boston, MA, Oct. 2014, pp. 1-5.

[46] A. Suntives and R. Abhari, "Experimental evaluation of high-speed data transmission in a waveguide-based interconnect," in *Proc. IEEE Electrical Performance of Electronic Packaging*, Scottsdale, AZ, Oct. 2006, pp. 269-272.